Delay-Tolerant Control Design for Semiconductor Optical Amplifiers

Baosen Zhang*, Scott B. Kuntze, Lacra Pavel and J. Stewart Aitchison

Abstract—Semiconductor Optical Amplifiers (SOAs) are versatile active photonic devices that can provide complex functions in photonic circuits, such as linear amplification. SOAs must be regulated due to their nonlinear nature. We consider the state space formulation of a linear SOA model to design and analyze controller schemes. We show that delay in the feedback path is of fundamental importance to the stability and performance of the SOA system. Due to the sub-nanosecond dynamics, the SOA system is a challenging system to control. We derive a design tradeoff on the feedback controller and delay stability margin of the closed-loop system. Different control schemes are then compared to show that a dual control scheme using a feedforward and a feedback controller offers the best performance.

I. Introduction

Semiconductor optical amplifiers (SOAs) are active nonlinear photonic devices that are becoming increasing prevalent in today's photonic circuits. SOAs are very fast (sub-nanosecond) devices that provide functions such as optical amplification [1]. Due to the nonlinear nature of the SOA, the amplification function is not ideal. In particular, there exists a significant amount of channel cross-talk: the output optical power cannot be maintained constant due the fact that all optical channels share the same inversion carrier density. Noise at the input and output terminals can also make it difficult to design practical devices with SOAs [2].

It was shown in [3]–[5] that a state model can be derived from the governing non-linear partial differential equations and channel cross-talk can be reduced by using state feedback. However, no feedback loop delay was considered in the analysis and design in [3]. The total controller delay in the feedback loop is of fundamental importance for two reasons: stability and fast control. Controller delay arises naturally due to photodetection delay, electronic circuits delay, and modulation delay. In practice, SOAs are used in optical communications circuits with sub-nanosecond pulses. Since SOAs have such fast dynamics, the closed loop system is only able to tolerate a certain amount of delay, called the delay margin of the system. Thus any controller must be fast enough so the delay in the feedback does not exceed the delay margin. Any feedback controller must also be faster
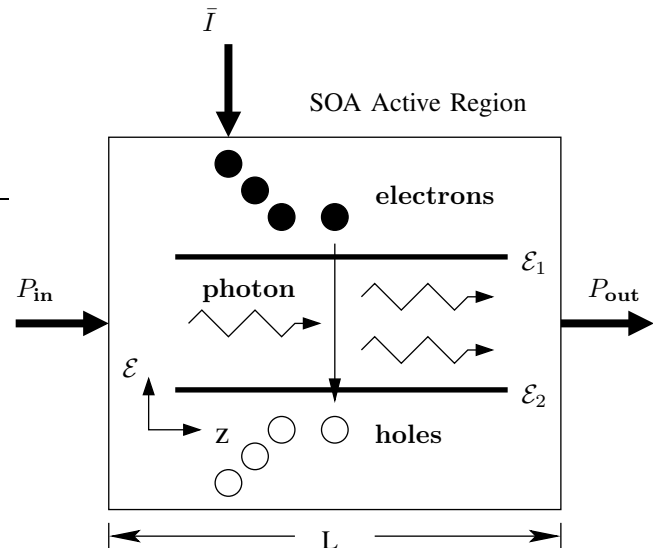
Fig. 1. Optical amplifications inside the SOA where $\mathcal{E}$ denotes energy. Current $\bar{I}$ supplies the electrons and holes. An incoming photon causes a stimulated recombination of a mobile electron and a hole, and two identical photons are released, therefore amplifying the input power along the length of the SOA.

than the pulse durations to have meaningful control of the output. This sensitivity of a SOA system to the speed of the controller presents a challenging control design problem due to the sub-nanosecond dynamics.

In this paper we analyze the effect of delay in the feedback path, starting from a complete model that includes the drive circuit and the parasitics (Section II). To do this we design optimal state feedback controllers and Kalman state estimators which can be used to the reject noise in the system (Section III), and then we analytically calculate the delay margin of the system. We thus show that the system is extremely sensitive to delay (Section IV), and therefore the feedback controller needs to be designed with rather demanding constraints. We show that the Frobenius norm of the controller can be used to effectively characterize this relationship between the stability delay margin and the feedback controller. Finally we present several alternative controllers (Section V) and show that a design that has both a feedforward and a feedback controller is the best performing one.

II. Model Derivation

A SOA is basically a laser diode without end mirrors, and the amplification of the input optical signals is essentially
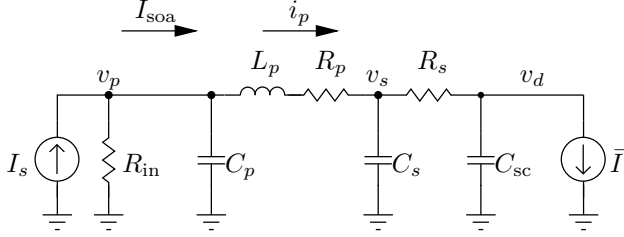
Fig. 2. SOA equivalent circuit model including both the drive circuit and the SOA electronic parasitics from [6]. All components are defined in Table I.

Parameter	Symbol	Value	Unit
Source current	I_s	—	mA
Source resistance	R_{in}	50	Ω
Package capacitance	C_p	10	pF
Package inductance	L_p	1	nH
Package resistance	R_p	1	Ω
Chip capacitance	C_s	3	pF
Chip resistance	R_s	1	Ω
Space-charge capacitance	C_{sc}	3	pF
Total active region current	$\bar{I}$	—	mA
Inversion carrier density	N	—	cm^{-3}
Active region current	I	—	mA
Recombination rate	R	—	cm^{-3}s^{-1}
Single-pass gain	g	—	cm^{-1}
Optical channel power	P	—	mW
ASE channel power	Q	—	mW
Length	L	500	μm
Interaction volume	V	120	μm^3
SOA cross-sectional area	A	0.24	μm^3
Optical carrier frequency	ω	1.22^{15}	rad/s
Waveguide loss	α	40	cm^{-1}
Zero-bias inversion density	N_e	5×10^{10}	cm^{-3}
Diode ideality factor	n	2	—
Temperature	T	300	K
Planck's constant	$\hbar$	1.054×10^{-34}	$J \cdot s$
Elementary charge	q	1.602×10^{-19}	C
Boltzmann constant	k_B	1.38×10^{-23}	J/K
Bias inversion density	N_0	3.8×10^{24}	m^{-3}
Bias current	I_0	0.150	mA
Bias total optical input	P_{in0}	1	mW

a function of the inversion carrier density $N(t)$ as shown in Fig. 1, where $N(t)$ is the number of electrons in upper energy level ($\mathcal{E}_1$) minus the number of electrons in the lower energy level ($\mathcal{E}_2$). A parasitic network lies between the current injected into the terminals of the SOA, I_s, and the current that reaches the active region, $\bar{I}$ [6]–[8]. The equivalent circuit is shown in Fig. 2 with components defined in Table I.

A. Governing Equations and Driver Circuit

The SOA is governed by the following set of equations [9]: the inversion carrier density rate equation,

$$
N(z,t)t = \frac{I(z,t)}{qV} - R(N,z,t)
$$
$$
- \frac{1}{A} \sum_{i=0}^{m} \frac{g_i\big(N(z,t), P(z,t), Q^{\pm}(z,t)\big)}{\hbar\omega_i} P_i(z,t)
$$
$$
- \frac{2}{A} \sum_{j=1}^{\mu} \frac{g_j\big(N(z,t), P(z,t), Q^{\pm}(z,t)\big)}{\hbar\omega_j} \big(Q_j^+(z,t) + Q_j^-(z,t)\big)
$$
(1)

the set of signal propagation equations,

$$
\frac{\partial P_i(z,t)}{\partial z} = g_i\big(N(z,t), P(z,t)\big) P_i(z,t) - \alpha_i P_i(z,t), \quad (2)
$$

and the set of amplified spontaneous emission (ASE) propagation equations,

$$
\frac{\partial Q_j^{\pm}(z,t)}{\partial z} = \pm g_j\big(N(z,t), P(z,t), Q^{\pm}(z,t)\big) Q_j^{\pm}(z,t)
$$
$$
\mp \alpha_j Q_j^{\pm}(z,t) + \hbar\omega_j R_{sp,j},
$$
(3)

where i ranges over the number of optical channels, j ranges over the number of ASE channels, $N(t)$ is the inversion carrier density and all other parameters are given in Table I. We take the states of the system to be $\mathbf{z}(t) = \begin{bmatrix} v_p(t) & i_p(t) & v_s(t) & N(t) \end{bmatrix}^T$. The non-linear state equations are derived in [4] using length-averaging and verified experimentally in [5]. The state equations are restated here for convenience:

$$
\dot{v}_p = \frac{v_p}{R_{in}C_p} \frac{i_p}{C_p} + \frac{I_s}{C_p} \tag{4a}
$$

$$
\dot{i}_p = \frac{v_p}{L_p} - \frac{R_p i_p}{L_p} - \frac{v_s}{L_p} \tag{4b}
$$

$$
\dot{v}_s = \frac{i_p}{C_s} - \frac{v_s}{R_s C_s} + \frac{\frac{n k_B T}{q} \ln\left(\frac{N}{N_e} + 1\right)}{R_s C_s} \tag{4c}
$$

$$
\dot{N} = \left[C_{sc} \frac{n k_B T}{q} \ln\left(\frac{N}{N_e} + 1\right) N + qV \right]^{-1} \left[\frac{v_s}{R_s} \right.
$$
$$
- \frac{\frac{n k_B T}{q} \ln\left(\frac{N}{N_e} + 1\right)}{R_s} - qV\bar{R}
$$
$$
- qL \sum_{i=0}^{m} \left(\frac{P_{out,i} - P_{in,i}}{\hbar\omega_i L} + \frac{\alpha_i \bar{P}_i}{\hbar\omega_i} \right)
$$
$$
\left. - 4qL \sum_{j=1}^{\mu} \left(\frac{Q_j(L) - Q_j(0)}{\hbar\omega_j L} + \frac{\alpha_j \bar{Q}_j^+}{\hbar\omega_j} \right) \right].
$$
(4d)

B. Linear Model

The linearization of the nonlinear equations results in a state space model as:

$$
\dot{\mathbf{z}} = \mathbf{F}\mathbf{z} + \mathbf{G}\mathbf{u} \tag{5a}
$$

$$
\mathbf{v} = \mathbf{H}\mathbf{z} + \mathbf{J}\mathbf{u}, \tag{5b}
$$

4155

where $\mathbf{z}$ is the state vector in (4), $\mathbf{u}$ is the input vector composed of

$$\mathbf{u} = \begin{bmatrix} I_s(t) & \mathbf{P}_{in}^T(t) \end{bmatrix}^T, \tag{6}$$

and $\mathbf{v}$ is the output vector composed of

$$\mathbf{v}(t) = \begin{bmatrix} I_{soa}(t) & \mathbf{P}_{out}^T(t) \end{bmatrix}^T \tag{7}$$

where $\mathbf{P}_{in}$ and $\mathbf{P}_{out}$ represents the total input and total output powers respectively. The algebraic expressions of matrix $\mathbf{F}$ is obtained by linearizing (4),

$$\mathbf{F} = \begin{bmatrix} -1/R_{\text{in}}C_p & -1/C_p & 0 & 0 \\ 1/L_p & -R_p/L_p & -1/L_p & 0 \\ 0 & 1/C_s & -1/R_sC_s & F_{3,4} \\ 0 & 0 & F_{4,3} & F_{4,4} \end{bmatrix}, \tag{8}$$

where

$$F_{34} = \frac{1}{R_sC_s}\frac{nk_BT}{q}\ln(\frac{N}{N_e}+1)N \tag{9a}$$

$$F_{43} = \frac{1}{(C_{\text{sc}}\frac{nk_BT}{q}\ln(\frac{N}{N_e}+1)/N + qV)R_s} \tag{9b}$$

$$F_{44} = -\frac{C_{\text{sc}}}{(C_{\text{sc}}\frac{nk_BT}{q}\ln(\frac{N}{N_e}+1)/N + qV)^2}\left[\frac{v_s}{R_s}\right.$$
$$-\frac{\frac{nk_BT}{q}\ln(\frac{N}{N_e}+1)}{R_s} - qVR$$
$$-qL\sum_{i=0}^{m}\left(\frac{P_{\text{out},i} - P_{\text{in},i}}{L} + \alpha\bar{P}_i\right)$$
$$\left. -4qL\sum_{j=1}^{\mu}\left(\frac{Q_{\text{out},j} - Q_{\text{in},j}}{L} + \alpha\bar{Q}_j\right)\right]^2\left[\right.$$
$$\left.\frac{nk_BT}{q}\ln\left(\frac{N}{N_e}+1\right)N^2\right] \tag{9c}$$
$$+\frac{1}{C_{\text{sc}}\frac{nk_BT}{q}\ln(\frac{N}{N_e}+1)/N + qV}\left[\right.$$
$$-\frac{1}{R_s}\frac{nk_BT}{q}\ln(\frac{N}{N_e}+1)N$$
$$-qVRN - qL\sum_{i=0}^{m}\left(\frac{1}{L}P_{\text{out},i}N + \alpha\bar{P}_iN\right)$$
$$\left. -4qL\sum_{j=1}^{\mu}\left(\frac{1}{L}Q_{\text{out},j}N + \alpha\bar{Q}_jN\right)\right],$$

and $\mathbf{G}$, $\mathbf{H}$, and $\mathbf{J}$ can be obtained similarly.

The numerical values matrices $\mathbf{F}$, $\mathbf{G}$, $\mathbf{H}$, and $\mathbf{J}$ are calculated around the bias point given in Table I,

$$\mathbf{F} = \begin{bmatrix} -2e^9 & -1e^{11} & 0 & 0 \\ 1e^9 & -1e^9 & -1e^9 & 0 \\ 0 & 3e^{11} & -3e^{11} & 4.7e^{-15} \\ 0 & 0 & 2e^{34} & -4.4e^{10} \end{bmatrix} \mathbf{G} = \begin{bmatrix} 1.0e^{11} & 0 \\ 0 & 0 \\ 0 & 0 \\ 0 & -4.9e^{36} \end{bmatrix}$$

$$\mathbf{H} = \begin{bmatrix} -0.02 & 0 & 0 & 0 \\ 0 & 0 & 0 & 3.7e^{-25} \end{bmatrix} \qquad \mathbf{J} = \begin{bmatrix} 1.0 & 0 \\ 0 & 102.5 \end{bmatrix}.$$

The linearized system can be easily checked to be controllable and obserservable. The linearized model has been
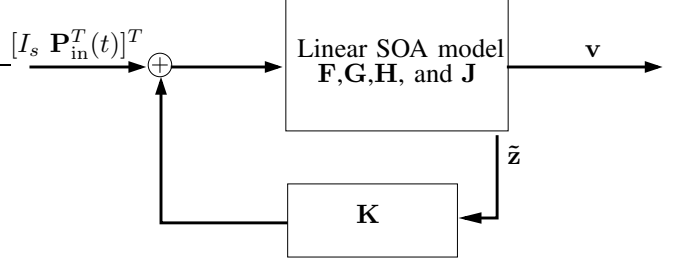

Fig. 3. A system view of the SOA and the feedback controller.

checked to be valid around the bias point for a 20% modulation in the input power, and its operation range expands when feedback is used [3]. It is important to note here that our analysis holds regardless of the actual number of optical channels in the SOA. The goal of the controller is to maintain the total output optical power constant when the input into the SOA changes or some input channels are dropped. This goal is equivalent to maintaining the inversion carrier density constant [3].

C. Model Scaling

Note that the system matrices $\mathbf{F}$, $\mathbf{G}$ and $\mathbf{H}$ are not numerically well conditioned. For example, the reciprocal condition number [10] of F is $\text{RCOND}(\mathbf{F}) = 5.2 \times 10^{-48}$. This numerical problem is general once the equivalent electronic circuit of the SOA is taken into account. To solve this, we use scaling. Specifically, if we look more closely at the eigenvalues of $\mathbf{F}$,

$$eig(F) = \begin{bmatrix} -3.3e^{11} & -2e^9 + 1e^{10}i & -2e^9 - 1e^{10}i & -4.3e^{10} \end{bmatrix} \tag{11}$$

since the eigenvalues of $\mathbf{F}$ are not far apart and so $\mathbf{F}$ is not a stiff matrix [11]. We use a simple diagonal scaling matrix T on the state vector, such that

$$\tilde{\mathbf{z}} = \mathbf{T}\mathbf{z} \tag{12}$$

where

$$\mathbf{T} = \begin{bmatrix} 1 & 0 & 0 & 0 \\ 0 & 1 & 0 & 0 \\ 0 & 0 & 1 & 0 \\ 0 & 0 & 0 & 10^{-25} \end{bmatrix}. \tag{13}$$

In the new coordinates, the linear representation is

$$\dot{\tilde{z}} = \tilde{\mathbf{F}}\tilde{\mathbf{z}} + \tilde{\mathbf{G}}\mathbf{u} \tag{14a}$$
$$\mathbf{v} = \tilde{\mathbf{H}}\tilde{\mathbf{z}} + \mathbf{J}\mathbf{u} \tag{14b}$$

where $\tilde{\mathbf{F}} = \mathbf{TFT}^{-1}$, $\tilde{\mathbf{G}} = \mathbf{TG}$, and $\tilde{\mathbf{H}} = \mathbf{HT}^{-1}$. With the new scaling $\text{RCOND}(\tilde{\mathbf{F}}) = 2.3 \times 10^{-3}$. From this we can see that after scaling the numerical conditioning of the system is much improved.

III. OPTIMAL CONTROL DESIGN

A. Optimal State Feedback

The general setup of the feedback controller is given in Fig 3. The goal of the feedback controller $\mathbf{K}$ is to keep the

inversion carrier level constant to suppress crosstalk. This controller can be generated using many standard techniques; here we choose to use optimal state feedback. In a real physical system not all states can be equally used to for feedback. For example, according to the circuit in Fig 2, only the state v_p is directly accessible, and the other states, i_p, v_s and N need to be estimated. Therefore, we want to rely more heavily on v_p then on the other states. Optimal control can be used to achieve the above criteria. The SOA here is modeled as a linear time-invariant system, so we use the well-known linear quadratic regular (LQR) design [12]. The optimal control problem is to find a controller, K, such that the cost function J

$$ J = \int_0^\infty (\tilde{\mathbf{z}}^T(t)\mathbf{Q}\tilde{\mathbf{z}}(t) + \mathbf{u}^T(t)\mathbf{R}\mathbf{u}(t))\,\mathrm{d}t \qquad (15) $$

is minimized, where $\mathbf{Q}$ is a positive semi-definite matrix representing the cost associated with the states, and $\mathbf{R}$ is a positive definite matrix representing the cost associated with the outputs. $\mathbf{K}$ is selected by solving the algebraic Riccati equation

$$ \tilde{\mathbf{F}}^T\mathbf{P} + \mathbf{P}\tilde{\mathbf{F}} - \mathbf{P}\tilde{\mathbf{G}}\mathbf{R}^{-1}\tilde{\mathbf{G}}^T\mathbf{P} + \mathbf{Q} = \mathbf{0}, \qquad (16) $$

where

$$ \mathbf{K} = -\mathbf{R}^{-1}\tilde{\mathbf{G}}^T\mathbf{P}. \qquad (17) $$

The efficiency of such a controller can be seen in Fig. 4 where we plotted the result for

$$ \mathbf{Q} = \begin{bmatrix} 1 & 0 & 0 & 0 \\ 0 & 10 & 0 & 0 \\ 0 & 0 & 10 & 0 \\ 0 & 0 & 0 & 10 \end{bmatrix}, \mathbf{R} = \begin{bmatrix} 1 & 0 \\ 0 & 1 \end{bmatrix}. \qquad (18) $$

The carrier density of the closed-loop system is almost constant compared to the carrier density of the open-loop system under 50% input optical power modulation as desired.

B. Observer

In the above section discussing state feedback, we have assumed that all the states would be available for feedback. This is not the case in practice. The only state directly accessible is v_p. The other electronic states i_p and v_s come from the small signal model of the driver electronics of the SOA, and are not accessible physical quantities. Also the inverse carrier density N is very difficult to measure. Therefore we must design a state observer as shown in Fig. 5.

Since both the input signal $\mathbf{u}$ and the output signal $\mathbf{v}$ are corrupted by noise, we need to use a noise rejection filter. With our state space model, we can use a Kalman filter that would reject the noise and give a good estimation of the states. The filter is set up as

$$ \dot{\tilde{z}} = \tilde{\mathbf{F}}\tilde{\mathbf{z}} + \tilde{\mathbf{G}}\tilde{\mathbf{u}} + \mathbf{B}\mathbf{w} \qquad (19a) $$

$$ \mathbf{v} = \tilde{\mathbf{H}}\tilde{\mathbf{z}} + \mathbf{J}\mathbf{u} + \mathbf{r}, \qquad (19b) $$
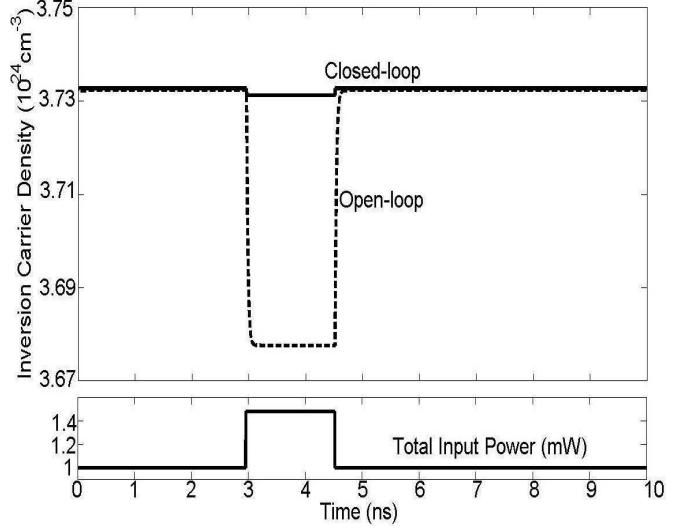

Fig. 4. Comparison of the closed-loop and open-loop system: top graph shows the changes in the inversion carrier density, and bottom graph shows the total input optical power.
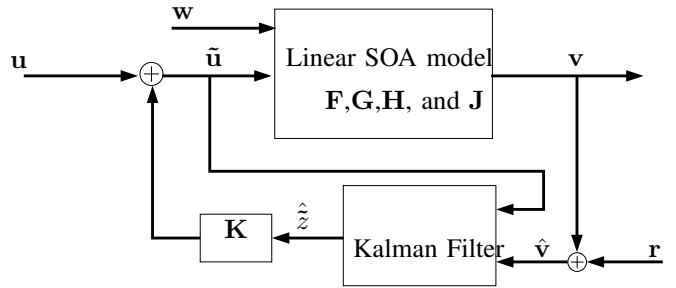

Fig. 5. Setup of the SOA state estimator.

where $\mathbf{w}$ and $\mathbf{r}$ are noises at the input and output of the SOA respectively. For simplicity of design, $\mathbf{w}$ and $\mathbf{r}$ are assumed to be uncorrelated wide-sense stationary vector Gaussian white noises with zero-mean. The estimation error is given by $e(t) = \tilde{z}(t) - \hat{\tilde{z}}(t)$. The Kalman filter can be easily designed by solving an algebraic Riccati equation and Fig. 6 shows the estimated state and the actual state. The estimated state tracks the actual state very well and is much less noisy.

IV. DELAY ANALYSIS

The SOA is useful in communications because its fast speed and small size. If state feedback is used, and all of the states except v_p are not directly accessible, the delay in the closed loop system in Fig. 3 becomes an important problem. In this section we show that delay is an important factor and might make state feedback impractical. Delay in this system arises out of two mechanisms, the first is from the signal propagation delay through the SOA and the second is the delay from the surrounding optoelectronics. The later delay arises naturally from the state observer circuits due to photoelectric conversion delay and electronic circuits delay. Since the optoelectronic delay is much larger than the signal propagation delay, the delays in the system term can be
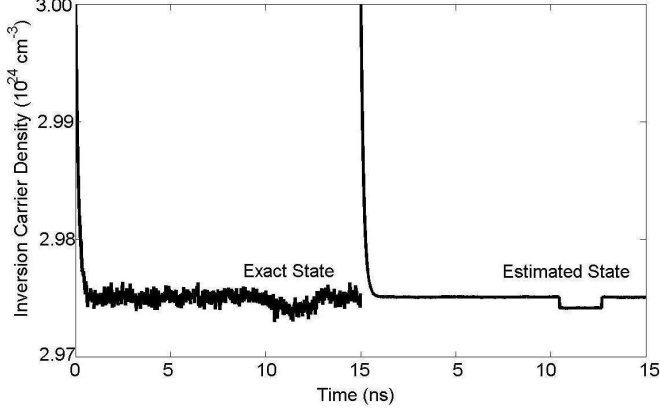
4157

Fig. 6. Comparison between the actual SOA state (solid line) and the estimated SOA state (dash line). Transients are included to show tracking.
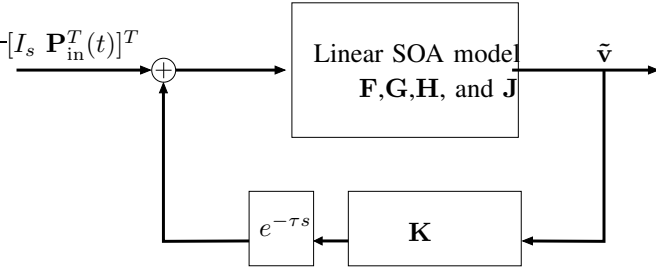

Fig. 7. Feedback loop with delay.

considered as a lumped delay as shown in (20). A block diagram representation is shown in the closed loop system in Fig. 7.

$$\dot{\tilde{z}} = \mathbf{A_0}\tilde{z} + \mathbf{A_1}\tilde{z}(t - \tau) + \tilde{\mathbf{G}}\mathbf{u}, \qquad (20)$$

where $\mathbf{A_0} = \tilde{\mathbf{F}}$ and $\mathbf{A_1} = \tilde{\mathbf{G}}\mathbf{K}$. Thus we can apply Theorem 2.13 in [13] to obtain necessary and sufficient conditions for delay stability. This theorem essentially gives a test for the delay in the feedback loop that would cause the poles (eigenvalues) of the closed-loop system to cross into the right half complex plane using constant matrices formed by the Kronecker tensor product. This theorem can be efficiently implemented numerically in Matlab based on the eigenvalues and generalized eigenvalues of constant matrices. It is stated here for convenience.

Theorem 1 (Constant Matrices Test): Suppose the system in (20) is stable at $\tau = 0$. Define $\bar{\tau}$ to be the the delay margin of the system. Define the matrices $\mathbf{B_0}, \mathbf{B_1},$ and $\mathbf{B_2} \in \mathbb{R}^{16 \times 16}$ by $\mathbf{B_1} = \mathbf{A_0} \oplus \mathbf{A_0^T}, \mathbf{B_0} = \mathbf{I} \otimes \mathbf{A_1^T},$ and $\mathbf{B2} = \mathbf{A_1} \otimes \mathbf{I}$. Furthermore, define

$$\mathbf{U} = \begin{bmatrix} I & 0 \\ 0 & B_2 \end{bmatrix} \quad \mathbf{V} = \begin{bmatrix} 0 & I \\ -B_0 & -B_1 \end{bmatrix}.$$

Then, $\bar{\tau} = \infty$ if $\sigma(\mathbf{U}, \mathbf{V}) \cap \partial\mathbb{D} = \emptyset$. If, however, $\sigma(\mathbf{U}, \mathbf{V}) \cap \partial\mathbb{D} \neq \emptyset$ and $eig(\mathbf{A_0} + \mathbf{A_1}z_i) = \{0\}$ for all $z_i \in \sigma(\mathbf{U}, \mathbf{V}) \cap \mathbb{D}$, then $\bar{\tau} = \infty$ as well. In these cases the system in (20) is stable

independent of delay. Otherwise,

$$\bar{\tau} = \min \frac{\theta_i}{\omega_i}, \qquad (21)$$

where $\theta_i \in [0, 2\pi], \omega_i \in \mathbb{R}^+, \omega_i \neq 0,$ and $e^{-j\theta_i} \in \sigma(\mathbf{U}, \mathbf{V})$ satisfy the relation $j\omega_i \in eig(\mathbf{A_0} + \mathbf{A_1}e^{-j\theta_i})$. The system in (20) is stable for all $\tau \in [0, \bar{\tau})$, but is unstable at $\tau = \bar{\tau}$. Here $\oplus$ denotes the Kronecker tensor sum, $\otimes$ denotes the Kronecker tensor product, $eig(\cdot)$ denotes the eigenvalues, $\sigma(\cdot, \cdot)$ denotes the generalized eigenvalues, and $\partial\mathbb{D}$ denotes the unit circle on the complex plane. ∎

For our system, the delay margin depends on the feedback controller $\mathbf{K}$ used. According to Thm 1, for a different $\mathbf{K}$, there would be an different $\mathbf{A_1}$, and thus a different delay margin. For example, the LQR controller used in Fig. 4 gives a delay margin of about 17.4 ps. It is very difficult to design a optoelectronic circuit with delay less than 17.4 ps, since a single gate delay in a NOT gate is around 4.5 ps [14], and the observer is likely much more complex since it needs to include detection, processing and optical modulation circuits.

In general, once a electronic circuit is chosen to implement the feedback controller $\mathbf{K}$, the delay in the circuit is known. However, a general method to design a feedback controller for a MIMO system to have a specific delay margin does not exist. Here we propose to use the Frobenius norm of the controller to characterize the overall strength of feedback, i.e.,

$$||K||_F^2 = \sum_{i=1}^{m} \sum_{j=1}^{n} |k_{ij}|^2 = trace(K^T K) = \sum_{i=1}^{\min(m,n)} \sigma_i^2 \qquad (22)$$

where σ_i terms denote the singular values of $\mathbf{K}$ and $\mathbf{K} \in \mathbb{R}^{m \times n}$. It is expected that the delay margin is inversely proportional to the strength of feedback ($||\mathbf{K}||_F$). To validate this hypothesis, optimal feedback controllers with different Frobenius norms are designed, the associated delay margins are calculated via Thm 1, and the results are plotted in Fig. 8. The controllers are generated using the LQR design by varying over different Q and R matrices and for simplicity, Q and R and kept as diagonal matrices. Fig. 8 is a log-log plot of about 1000 points with the delay margin $\bar{\tau}$ on the x-axis and the feedback controller $||\mathbf{K}||_F$ on the y-axis. This plot clearly shows that the delay margin is inversely proportional to the strength of the feedback controller $\mathbf{K}$. In fact, a simple function of the form $f(x) = ax^{-1} + b$ fits the curve with a R^2 of 99%. It should be noted that for large delay margins, the curve will become flat because there exists a threshold controller strength for which the delay margin becomes infinite.

The sensitivity of the SOA system to delay presents a challenging design problem because it puts some rather demanding constrains on the feedback controller. For example, for a delay margin of 50 ps, the maximum strength of the controller can have is 0.2. Fig. 8 gives the design tradeoff rule: if a large delay margin is required (due to a slow state estimator and controller), then the controller must be
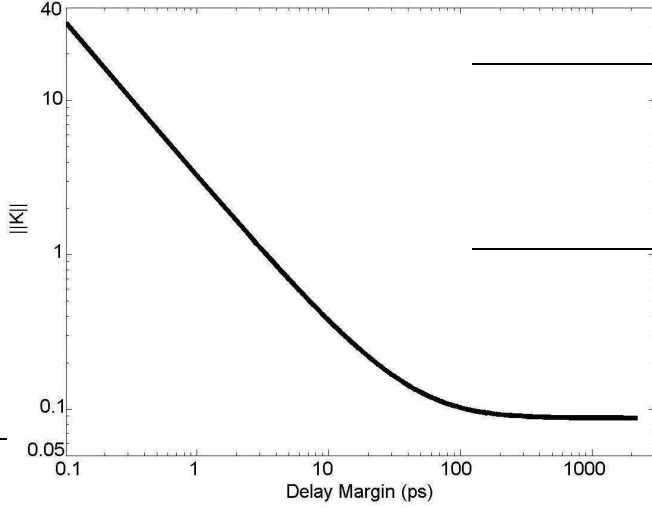
Fig. 8. Feedback controller norm against the delay margin on a log-log scale. A clear inverse relationship $f(x) = ax^{-1} + b$ is demonstrated. The line flats out for larger delay margins because the delay margin becomes infinite for controller norm less than a certain threshold.
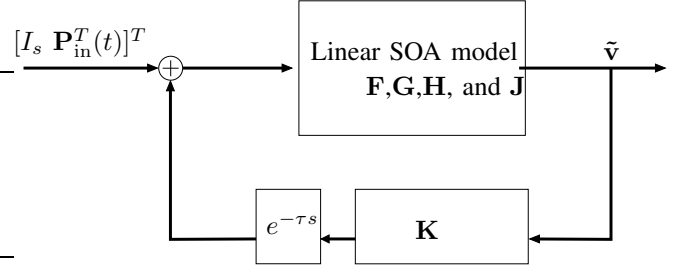

Fig. 9. Output feedback configuration with delay in the feedback path. $\tilde{\mathbf{v}}$ is assumed to be available for feedback.
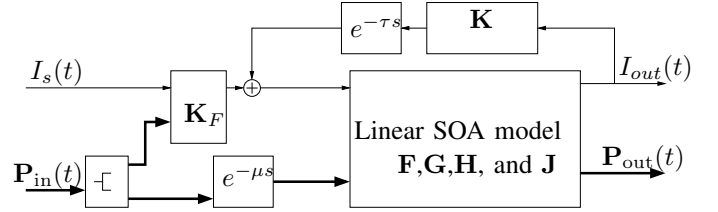

Fig. 10. Setup of the combined system involving both feedback and feedforward. Only the output current I_{out} is used in feedback for simplicity in physical implementations.

relatively weak in strength while still performing adequately; on the other hand, if a strong controller is needed, then fast state estimator and controller need to be designed to meet a more stringent delay margin. Analysis of this kind can be used in practice as a valuable design tool to trade feedback strength versus delay margin.

A. Output Feedback

If the output from the SOA is used as feedback instead of the states, then no estimation is needed since all optical outputs are available. However, delay is still present since there are conversions between optical and electrical signals, or at least in routing the optical signals to allow feedback. This problem can also be analyzed by using the state space model under the general delay framework established in (20) with the assumption that the SOA itself has negligible delay. This is equivalent to assuming that a change in the input $\mathbf{u}$ will produce an immediate change in the output $\mathbf{v}$ through the coupling matrix $\mathbf{J}$. For a typical SOA with a length of 500 microns and a relative index refraction of 3, the propagation time is 5 ps; this is much smaller than the delay in the feedback path, justifying the above assumption. With this assumption, the vector signal $\tilde{\mathbf{v}} = \mathbf{v} - \mathbf{J}\mathbf{u} = \tilde{\mathbf{H}}\tilde{\mathbf{z}}$ is available and can be feedback into the system. Considering the set up in Fig. 9, we can rewrite (20) as

$$\dot{\tilde{z}} = \mathbf{A_0}\tilde{\mathbf{z}} + \mathbf{A_1}\tilde{\mathbf{z}}(t - \tau) + \tilde{\mathbf{G}}\mathbf{u}, \qquad (23)$$

where $\mathbf{A}_0 = \tilde{\mathbf{F}}$ and $\mathbf{A}_1 = \tilde{\mathbf{G}}\mathbf{K}\tilde{\mathbf{H}}$. Thus only $\mathbf{A}_1$ needs to be changed in order to analyze delay in the output feedback case.

B. Feed-forward and Feedback

We can also use a feed-forward control scheme, which would be fast and delay-tolerant, but it needs the model

to match well with the physical SOA, which is unlikely to happen in practice. Output feedback is insensitive to modeling errors, but is intolerant to delay as shown in last section. Thus similar to erbium-doped fiber amplifier control in [15], we propose to combine both schemes to have fast regulator action and also insensitivity to SOA modeling errors. One such setup is shown in Fig 10, where both output feedback and feedforward controllers are used. In this setup, the input optical signal is split into two signals, with one entering the feedforward controller while the other one enters a delay loop represented by $e^{-\mu s}$, where μ is an delay to be designed such that the two input signals arrive in sync. The feedforward controller takes $\mathbf{P}_{in}$ and $\mathbf{I}_s$ and adjust the bias current of the SOA accordingly, i.e. to maintain $N(t)$ constant. This is further supplemented by a feedback signal of the output current I_{out} that is directly accessible so that no additional optoelectronics are needed. Furthermore, the feedback controller $\mathbf{K}$ can be simply proportional, leading to a simple physical implementation.

The closed-loop general system in Fig. 10 is described by (24),

$$\dot{\tilde{z}} = \mathbf{A_0}\tilde{\mathbf{z}} + \mathbf{A_1}\tilde{\mathbf{z}}(t - \tau) + \tilde{\mathbf{G}}\mathbf{K}_F\mathbf{u} \qquad (24)$$

which is essentially (23) with $\mathbf{u}$ replaced by $\mathbf{K}_F\mathbf{u}$ everywhere.

Fig 11(b) compares the performances of different control schemes. The delay in the feedback path τ is 100 ps. Since only the output current is fed back into the input current, a 100 ps delay is reasonable. The input consists of optical signals with sharp pulses and a slow sinusoidal variation over a longer time scale as shown in Fig. 11(a). Feedforward-only control reduces the the fast transients in the carrier density, but does not reduce the long-term variations. On the
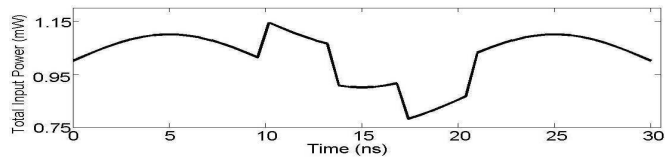
(a) Input test signal: the sinusoidal component represents the large time-scale power drift and the pulses represent data signals.
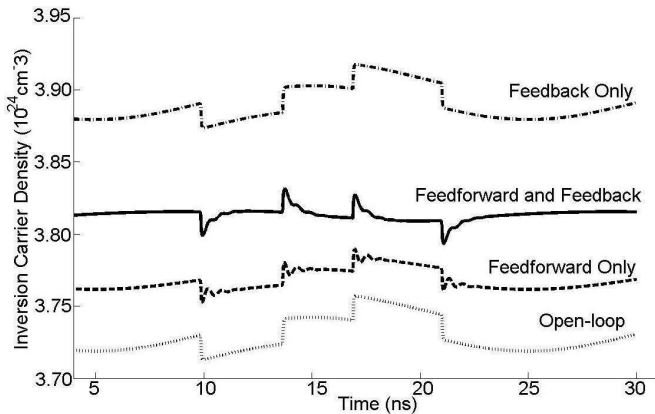
(b) Results of various control schemes for input test signal in (a). The mixed control scheme of both feedforward and feedback loops performs the best by keeping inversion carrier density relatively flat. The offset in the inversion carrier curves are caused by different biasing in the input current, and it is adjusted such that all curves are easily visible.

Fig. 11.   Input and the responses of the different controllers.

other hand, feedback-only control does not perform better than the open-loop system due to the weak control signal that is limited by the delay margin. The mixed configuration of feedforward and feedback performs much better than the others, giving a relatively flat carrier density profile.

V. Conclusions

We used a state space model to design and analyze various controllers for the SOA. In particular, delay in the feedback loop is shown to be of fundamental importance to the stability of the closed-loop system. We showed that the Frobenius norm can be used to effectively characterize the relationship between the feedback controller and the delay margin in the system. This framework gives a practical method of trading controller strength and delay margin in design. We then proposed different controller schemes that can work around the closed-loop delay stability problem. We showed that a dual control scheme of a feedforward controller together with a purely electronic feedback controller gives the best performance.

References

[1] K. D. LaViolette, "The use of semiconductor-optical-amplifiers for long optical links in the catv upstream optical network," IEEE Photon. Technol. Lett., vol. 10, 1998.

[2] P. Morel, A. S. R. Brenot, and B. Thedrez, "Wideband gain and noise figure modelling in soa," Optical and Quantum Electronics, vol. 38, 2006.

[3] S. B. Kuntze, L. Pavel, and J. S. Aitchison, "Controlling a semiconductor optical amplifier using a state-space model," IEEE Journal of Quantum Electronics, vol. 43, 2007.

[4] S. B. Kuntze, L. Pavel, and J. S. Aitchison, "Novel gain control in a multichannel semiconductor optical amplifier with equivalent circuit using nonlinear state-space methods," To Appear In Proc. IEEE Broadnets, Sep 2007.

[5] S. B. Kuntze, A. J. Zilkie, L. Pavel, and J. S. Aitchison, "Nonlinear state-space model of semiconductor optical amplifiers with gain compression for system design and analysis," IEEE J. Lightwave Technol., 2008. Accepted.

[6] R. S. Tucker, "High-speed modulation of semiconductor lasers," IEEE J. Lightwave Technol., vol. LT-3, 1985.

[7] R. S. Tucker and D. J. Pope, "Microwave circuit models of semiconductor injection lasers," IEEE Trans. Microwave Theory Technol., vol. MTT-31, 1983.

[8] R. S. Tucker and I. P. Kaminow, "High-frequency characteristics of directly modulated ingaasp ridge waveguide and buried heterostructure lasers," IEEE J. Lightwave Technol., vol. LT-2, 1984.

[9] J. Mork, A. Mecozzi, and G. Eisenstein, "The modulation response of a semiconductor laser amplifier," IEEE J. Select. Topics Quantum Electron., vol. 5, 1999.

[10] Golub and V. Loan, Matrix Computations. Johns Hopkins University Press, third ed., 1996.

[11] J. S. Ruiz and F. J. S. Bernabe, "A numerical study of stiffness effects on some high order splitting methods," Revista Mexicana de Fisica, vol. 52, 2006.

[12] L. S. Pontryagin, V. G. Boltranskii, R. V. Gamkrelidze, and E. F. Mishchenko, The Mathematical Theory of Optimal Processes. Wiley-Interscience, 1962.

[13] K. Gu, V. L. Kharitonov, and J. Chen, Stability of Time-Delay Systems. Birkhuser, 2003.

[14] L. Rodoni, F. Ellinger, and H. Jackel, "Ultrafast cmos inverter with 4.7 ps gate delay fabricated on 90nm soi technology," Electronic Letters, 2004.

[15] L. Pavel, "Control design for transient power and spectral control in optical communication networks," Proceedings of 2003 IEEE Conference on Control Applications, 2003.